

---

# HOTA: Hamiltonian framework for Optimal Transport Advection

---

**Nazar Buzun**  
CILAB.AI\*  
n.buzun@cilab.ai

**Daniil Shlenskii**  
CILAB.AI\*  
d.shlenskii@cilab.ai

**Maxim Bobrin**  
CILAB.AI\*  
m.bobrin@cilab.ai

**Dmitry V. Dylov**  
CILAB.AI\*  
d.dylov@cilab.ai

## Abstract

Optimal transport (OT) has become a natural framework for guiding the probability flows. Yet, the majority of recent generative models assume trivial geometry (e.g., Euclidean) and rely on strong density-estimation assumptions, yielding trajectories that do not respect the true principles of optimality in the underlying manifold. We present Hamiltonian Optimal Transport Advection (HOTA), a Hamilton–Jacobi–Bellman based method that tackles the dual dynamical OT problem explicitly through Kantorovich potentials, enabling efficient and scalable trajectory optimization. Our approach effectively evades the need for explicit density modeling, performing even when the cost functionals are non-smooth. Empirically, HOTA outperforms all baselines in standard benchmarks, as well as in custom datasets with non-differentiable costs, both in terms of feasibility and optimality.

## 1 Introduction

*Static (Monge-Kantorovich)* optimal transport was originally considered as the main framework for comparing and finding a cost-minimizing coupling between distributions [Villani et al., 2008], while optimality was mainly measured through the boundary marginals. Development of efficient and scalable OT solvers [Cuturi, 2013, Peyré et al., 2019] popularized OT across different areas, such as generative modeling [Makkuva et al., 2020, Korotin et al., 2022, Buzun et al., 2024], computational biology [Bunne et al., 2022], graphics [Bonneel and Digne, 2023], high-energy physics [Nathan T. Suri, 2024], and reinforcement learning [Klink et al., 2022, Asadulaev et al., 2024, Bobrin et al., 2024, Rupf et al., 2025]. However, one crucial limitation of static formulation is its inability to produce non-straight paths, which completely ignores the underlying geometry of the manifold of the data. In classical OT, the underlying geometric structure is solely determined by the choice of cost function (e.g., Euclidean distance), inherently limiting the capacity for fine-grained control over the trajectories. We refer to [Montesuma et al., 2024, Pereira and Amini, 2025] for recent overview of practical applications of OT and to Villani et al. [2008], Santambrogio [2015], Peyré et al. [2019] for a formal treatment.

On the other hand, the *dynamical* optimal transport paradigm, developed by Benamou and Brenier [2000], recasts static OT as a continuous-time variational problem on the space of probability paths, effectively incorporating time variable and enabling more nuanced control over optimal trajectories (e.g., through velocity, acceleration, length, or energy over the paths). Importantly, such formulation enables one to directly operate on manifolds of non-trivial geometry, whenever the underlying space contains curvature, obstacles, or is defined through potentials. This formulation is closely connected to stochastic optimal control (SOC), where trajectories are stochastic yet must still maintain optimality,

---

\*Computational Imaging Lab

a problem class known as the generalized Schrödinger bridge (GSB) Liu et al. [2024], Bartosh et al. [2024],.

A common strategy for GSB involves solving the dual formulation via Hamilton-Jacobi-Bellman (HJB) equations, which provide a flexible and a theoretically grounded framework for deriving optimal trajectories (Liu et al. [2022], Neklyudov et al. [2024]). These methods parameterize the cost through a Lagrangian, enforcing optimality via the preservation of kinetic energy or using other path-based penalties. While HJB-based approaches yield theoretically sound solutions, they suffer from critical drawbacks: (1) unstable optimization dynamics, leading to high-variance gradients and poor sample efficiency in high dimensions, and (2) the absence of a strict terminal distribution matching criterion, resulting in inexact couplings. Additionally, they typically require differentiable Lagrangians, restricting applicability to smooth costs only.

In the current work, we study the Generalized Schrödinger Bridge problem between two measures, where the underlying geometry is defined through potentials. We propose a new HJB-based framework that explicitly solves GSB task, resolves the learning stability problems of the previous approaches, and has theoretical guarantees. We conduct extensive empirical evaluations on existing low-dimensional physically-inspired benchmarks, as well as in the high-dimensional generative setting. In short, our contributions are as follows:

- Hamiltonian dual reformulation of dynamical OT that binds Kantorovich potentials with an HJB value function, yielding a density-free objective and providing the performance gain compared to existing works;
- Proposed approach is robust to complex geometries and works even with non-smooth cost functions as the proposed objective explicitly incorporates the potential term;
- HOTA attains state-of-the-art empirical results in a diverse set of tasks, demonstrating both better feasibility (exact marginal matching) and optimality (cost along trajectories) compared to current dynamic OT solvers.

## 2 Related work

**Diffusion Models and Matching Algorithms.** Diffusion models have emerged as powerful tools for generative modeling by prescribing the time evolution of marginal distributions. Matching algorithms, such as Action Matching (Neklyudov et al. [2024]) and Flow Matching (Lipman et al. [2023]), learn stochastic differential equations (SDEs) that align with prescribed probability paths [Blessing et al., 2025]. These methods typically assume explicit or implicit intermediate densities of the flow, whereas our approach (HOTA) optimizes a complete stochastic path from source to target distributions.

**Generalized Schrödinger Bridge.** The GSB problem extends SB by introducing state costs that penalize or reward specific trajectories (Chen et al., 2015). Prior methods for solving GSB, such as DeepGSB (Liu et al. [2022]), often relax feasibility constraints or rely on Sinkhorn-based approximations, which can lead to instability or suboptimal solutions.

A recent approach GSBM [Liu et al., 2024] follows an alternating optimization scheme: in the first stage, it learns the drift field  $v_t$  while keeping the marginal distributions  $\rho_t(x_t)$  fixed, using a Flow Matching-style objective. In the second stage, it updates the marginals conditioned on the boundary-coupled distribution  $\rho_t(x_t | x_0, x_1)$ , which is defined via the previously learned drift. While GSBM demonstrates strong empirical performance, it imposes two critical limitations: 1) it requires the state cost function  $U(x_t)$  to be differentiable everywhere, and 2) it assumes that the conditional marginals  $\rho(x_t | x_0, x_1)$  are Gaussian. The first constraint restricts the method’s applicability to domains with smooth geometries, sometimes mitigated via interpolation [Kapusniak et al., 2024], while the second can lead to suboptimal solutions, unless  $U_t$  function is not quadratic.

**Stochastic Optimal Control.** The connection between GSB and stochastic optimal control (SOC) has been explored in prior works (Theodorou et al. [2010]; Levine [2018]). SOC formulations often relax hard distributional constraints into soft terminal costs, which can introduce bias or require adversarial training (Liu et al. [2022]). Recently introduced Adjoint Matching approach [Domingo-Enrich et al., 2024a] and Stochastic Optimal Control matching (SOCM) [Domingo-Enrich et al., 2024b] address several existing limitations, but still produce highly unstable variance estimations. Our method provides a natural way to preserve the feasibility via Kantorovich potential sum.

### 3 Preliminaries

Consider stochastic process with controlled drift and diffusion:

$$dx_t = v(t, x_t) dt + \sigma(t, x_t) dW_t \quad (1)$$

where  $v : [0, 1] \times \mathbb{R}^d \rightarrow \mathbb{R}^d$  is the drift (control),  $\sigma : [0, 1] \times \mathbb{R}^d \rightarrow \mathbb{R}$  is the diffusion coefficient,  $W_t$  is  $d$ -dimensional Brownian motion. We solve the OT minimization task with marginal distributions  $(\alpha, \beta)$  and dynamic cost functions  $c(x, \mu)$  and stochastic transport mapping  $\mu : \mathbb{R}^d \rightarrow \mathcal{P}(\mathbb{R}^d)$  presented in paper [Korotin et al. \[2022\]](#)

$$c(x, \mu) = \inf_{v(t, x) : x_0 = x, x_1 \sim \mu} \int_0^1 \mathbb{E} \mathcal{L}(t, x_t, v_t) dt, \quad \mathcal{L}(t, x_t, v_t) = \frac{\|v_t\|^2}{2} + U(x_t). \quad (2)$$

This problem is also known as generalized Schrödinger bridge (GSB). It is an extension of the classical Schrödinger Bridge (SB) problem, which is a distribution-matching task seeking a diffusion model that transports an initial distribution  $\alpha$  to a target distribution  $\beta$ . While the standard SB minimizes the kinetic energy ( $L^2$  cost in OT), the GSB introduces additional flexibility by incorporating a state cost  $U(x_t)$ , allowing for more general optimality conditions beyond just kinetic energy minimization. The standard SB's reliance on kinetic energy (Euclidean cost) may not be ideal for all applications (e.g., image spaces, where distance may not be meaningful). Many scientific domains (population modeling, robotics, molecular dynamics) require richer optimality conditions, which GSB accommodates via  $U(x_t)$ . The potential term usually characterizes the geometry of the space. But in addition, we can also include some physical properties of the flow, e.g., entropic penalty or “mean-field” interaction [\[Liu et al., 2022\]](#). Thus, the optimal trajectories are curved to avoid regions with high values of  $U(x_t)$ .

Neural networks can effectively solve high-dimensional Optimal Transport (OT) problems by learning the Kantorovich potentials, which maximizes the dual objective [\(Korotin et al. \[2022\], Buzun et al. \[2024\]\)](#). It is shown in [Villani et al. \[2008\]](#) (Theorem 5.10) that OT task is equivalent to the maximization of the Kantorovich potentials sum:

$$\sup_{g \in L_1(\beta)} \left[ \mathbb{E}_\alpha[g^c(x)] + \mathbb{E}_\beta[g(y)] \right], \quad (3)$$

where  $g^c$  denotes  $c$ -conjugate transform of the potential  $g$ :

$$g^c(x) = \inf_{\mu(x) : \mathbb{R}^d \rightarrow \mathcal{P}(\mathbb{R}^d)} \mathbb{E}_{y \sim \mu(x)} \left[ c(x, \mu) - g(y) \right]. \quad (4)$$

Here  $\mu(x)$  is the stochastic transport mapping, and in our notation it is the final distribution of the stochastic process  $x_1$  under condition that  $x_0 = x$ . The marginality requirement of the final distribution of  $x_1$  (which must correspond to  $\beta$ ) is ensured by the potential difference  $\mathbb{E}_\beta g(y)$  and  $\mathbb{E}_\alpha \mathbb{E}_{y \sim \mu(x)} g(y)$ , which tends to infinity otherwise.

But unlike classical OT, we need to minimize the cost throughout the trajectory  $x_t, t \in [0, 1]$  with the following objective

$$g^c(x) = \inf_{v(x, t)} \mathbb{E} \left[ \int_0^1 \left( \frac{\|v(t, x_t)\|^2}{2} + U(x_t) \right) dt - g(x_1) \middle| x_0 = x \right]. \quad (5)$$

In the last expression, we have united infimums by  $\mu(x)$  and control  $v(t, x)$  and as a sequence have removed the right side condition  $x_1 \sim \mu(x)$ . Based on dynamic programming approach, define the value function. For any  $0 \leq t \leq 1$ , the value function satisfies:

$$s(t, x) = \inf_{x_t} \mathbb{E} \left[ \int_t^1 \left( \frac{\|v(t, x_t)\|^2}{2} + U(x_t) \right) dt - g(x_1) \middle| x_t = x \right], \quad (6)$$

such that our objective equals  $s(0, x)$  and the boundary condition at time point  $t = 1$  is

$$\forall x \in \mathbb{R}^d : s(1, x) = -g(x).$$

Function  $s(t, x)$  solves the Hamilton-Jacobi-Bellman (HJB) differential equation and it in turn allows us to find the conjugate potential  $g^c$  (4).

$$-\partial_t s(t, x) = \inf_v \{v^T \nabla_x s(t, x) + \mathcal{L}(t, x, v)\} + \frac{\sigma^2}{2} \text{tr}\{\nabla^2 s(t, x)\}. \quad (7)$$

Representation of the Lagrange function as a sum of kinetic and potential energy allows us to find the minimum in velocity ( $v$ ) in explicit form, such that  $v_t = -\nabla_x s(t, x_t)$ . Together with potential optimization (3), we obtain the final GSB objective in dual Kantorovich form. We provide a detailed proof in Appendix section B.

**Theorem 1** (Dual GSB problem). *Given distributions  $\alpha, \beta \in \mathcal{P}(\mathbb{R}^d)$  and stochastic dynamics (1) with cost functional (2), the dynamic optimal transport problem admits the following formulation:*

$$\max_{s(1, \cdot) \in L_1(\beta)} \{\mathbb{E}_\alpha s(1, x_1) - \mathbb{E}_\beta s(1, y)\} \quad (8)$$

where  $s(t, x) \in C^{1,2}([0, 1] \times \mathbb{R}^d)$  and satisfies HJB PDE  $\forall t \in [0, 1]$  and  $\forall x \in \mathbb{R}^d$

$$-\partial_t s(t, x) = -\frac{1}{2} \|\nabla_x s(t, x)\|^2 + U(x) + \frac{\sigma^2}{2} \text{tr}\{\nabla^2 s(t, x)\}. \quad (9)$$

The first expression in Theorem 1 plays the role of a discriminator and guarantees matching the target distribution  $\beta$ , and the second one is responsible for the optimality of trajectories. For the HJB equation to have a unique solution (in the viscosity sense), we require *coercivity* (Theorem 4.1 [Fleeting and Soner, 2006]) of the Hamiltonian for some constants  $C_1 > 0$  and  $C_2 \geq 0$

$$H(x, \nabla s, \nabla^2 s) = \frac{1}{2} \|\nabla_x s\|^2 - U(x) - \frac{\sigma^2}{2} \text{tr}\{\nabla^2 s\} \quad (10)$$

$$\geq C_1(\|\nabla s\|) - C_2(1 + \|x\| + \|\nabla^2 s\|) \quad (11)$$

The term  $\|\nabla_x s\|^2$  dominates for large values, so in case  $U(x)$  is bounded and  $\sigma > 0$  the solution is unique. By means of the optimized function  $s(t, x)$  we can generate the OT trajectories using Euler-Maruyama algorithm:

$$x_{t+\Delta t} = -\nabla_x s(t, x_t) \Delta t + \sigma \Delta W, \quad x_0 \sim \alpha. \quad (12)$$

Unlike most other methods, here we do not need to model the intermediate density of the  $x_t$  ( $t \in (0, 1)$ ) distribution, which greatly simplifies the learning process, but we need to store the generation history in a replay buffer for more stable HJB optimization in high-dimensional spaces.

## 4 Method

To find a stable and balanced solution  $s(t, x)$  for the given dynamic OT problem (1), we can follow a composite approach that combines optimal control (via HJB PDE constraints) and RL techniques (policy-based trajectory optimization). We approximate the value function using a parametric model  $s_\theta(t, x)$ . We have to maximize the potential matching functional (8) subject to the constraint that  $s_\theta(t, x)$  satisfies the HJB PDE. For that divide the time interval  $[0, 1]$  into  $T$  time steps and simulate  $n$  trajectories  $\{t_0^k, x_0^k, \dots, t_T^k, x_T^k\}_{k=1}^n$  using initial  $\alpha$  distribution and Euler-Maruyama method (12). Sample also  $n$  points  $y_k$  from the target distribution  $\beta$  and compute the potential matching loss as

$$L_{\text{pot}}(s_\theta) = \frac{1}{n} \sum_{k=1}^n s_\theta(1, x_T^k) - \frac{1}{n} \sum_{k=1}^n s_\theta(1, y^k). \quad (13)$$

The HJB PDE must hold for all  $t \in [0, 1]$  and  $x \in \mathbb{R}^d$ , but in practice, for more effective training, the training data should be sampled in the region of the flow (trajectories) concentration (according to Liu et al. [2022]). We enforce this by linear interpolation between datasets from  $\alpha$  and  $\beta$  as a rough estimation of the flow region and subsequently use the replay buffer  $\mathcal{B}$  to collect points from the previously obtained trajectories. Using data samples  $\{t^k, x^k\}_{k=1}^n$  from  $\mathcal{B}$  or the linear interpolation we compute HJB residual loss as

$$L_{\text{hjb}}(s_\theta, \bar{s}) = \frac{1}{n} \sum_{k=1}^n \left( \frac{\partial s_\theta^k}{\partial t} - \frac{1}{2} \|\nabla_x \bar{s}^k\|^2 + U(x^k) + \frac{\sigma^2}{2} \text{tr}\{\nabla^2 \bar{s}^k\} + \lambda_a \|a^k\| \right)^2 \quad (14)$$

$$+ \frac{1}{n} \sum_{k=1}^n \left( \frac{\partial \bar{s}^k}{\partial t} - \frac{1}{2} \|\nabla_x s_\theta^k\|^2 + U(x^k) + \frac{\sigma^2}{2} \text{tr}\{\nabla^2 s_\theta^k\} + \lambda_a \|a^k\| \right)^2, \quad (15)$$

where  $s_\theta^k = s_\theta(t^k, x^k)$ ,  $\bar{s}^k = \bar{s}(t^k, x^k)$  denotes the target model with EMA parameters,  $a^k$  is angular acceleration defined as

$$a^k = \frac{d}{dt} \frac{\nabla s_\theta(t^k, x^k)}{\|\nabla s_\theta(t^k, x^k)\|}. \quad (16)$$

The angular acceleration with coefficient  $\lambda_a$  forces the straightening of the trajectories (optionally). We divide the model into  $s_\theta$  and  $\bar{s}$  as it usually done in RL methods to make the optimization problem more similar to regression.

In the result, our model is trained on two criteria ( $L_{\text{pot}}$  and  $L_{\text{hjb}}$ ) simultaneously and to balance both impacts we scale the gradients of the hjb-loss and sum it with the pot-loss:

$$\nabla_\theta L_{\text{pot}}(s_\theta) + \lambda_{\text{hjb}} \text{EMA} \left( \frac{\|\nabla_\theta L_{\text{pot}}(s_\theta)\|}{\|\nabla_\theta L_{\text{hjb}}(s_\theta, \bar{s})\|} \right) \nabla_\theta L_{\text{hjb}}(s_\theta, \bar{s}). \quad (17)$$

The complete method is implemented as shown in Algorithm 1. It effectively combines the theoretical guarantees of optimal transport with the flexibility of neural network approximations, while maintaining numerical stability through careful gradient management. The adaptive balancing of the potential matching and HJB residual losses ensures stable convergence to a solution that satisfies both the optimality conditions and the boundary constraints.

---

**Algorithm 1** HOTA: Hamiltonian framework for Optimal Transport Advection

---

```

1: Input: value model  $s_\theta$ , model optimizer  $s_{\text{opt}}$ , distributions  $\alpha$  and  $\beta$ , potential function  $U(x)$ , diffusion coefficient  $\sigma$ .
2: Hyperparameters: train steps  $N$ , interpolation sample steps  $N_0$ , temporal discretization  $T$ , batch size  $n$ , hjb-loss weight  $\lambda_{\text{hjb}}$ , acceleration coefficient  $\lambda_a$ , learning rate lr, gradients scale EMA coefficient  $\tau$ .
3: Initialize target model  $\bar{s}$ ; replay buffer  $\mathcal{B} \leftarrow \emptyset$ ; gradients scale  $\alpha \leftarrow 1.0$ 
4: for iteration  $i = 1$  to  $N$  do
5:   Sample train data  $\{x_0^k\}_{k=1}^n \sim \alpha$ ;  $\{y^k\}_{k=1}^n \sim \beta$ 
6:   if  $i < N_0$  then
7:     Sample times  $\{t^k\}_{k=1}^n \sim U(0, 1)$ 
8:     For  $1 \leq k \leq n$  set  $x^k = x_0^k \cdot (1 - t^k) + y^k \cdot t^k$ 
9:   else
10:    Sample  $\{t^k, x^k\}_{k=1}^n \sim \mathcal{B}$ 
11:   end if
12:   Generate  $n$  trajectories  $\{t_0^k, x_0^k, \dots, t_T^k, x_T^k\}_{k=1}^n$  using current policy  $v_t = -\nabla s(t, x)$ 
13:   Add the 1-st trajectory  $\{t_0^0, x_0^0, \dots, t_T^0, x_T^0\}$  to  $\mathcal{B}$ 
14:   Compute gradients:
15:    $g_{\text{hjb}} = \nabla_\theta L_{\text{hjb}}(s_\theta, \bar{s}, \{t^k, x^k\}_{k=1}^n)$ 
16:    $g_{\text{pot}} = \nabla_\theta L_{\text{pot}}(s_\theta, \{x_T^k\}_{k=1}^n, \{y^k\}_{k=1}^n)$ 
17:   Update Parameters:
18:   Compute norms  $G_{\text{hjb}} = \|g_{\text{hjb}}\|_2$  and  $G_{\text{pot}} = \|g_{\text{pot}}\|_2$ 
19:   EMA update of gradients scale  $\alpha = \tau G_{\text{pot}} / G_{\text{hjb}} + (1 - \tau) \alpha$ 
20:   Sum the gradients  $g = g_{\text{pot}} + \lambda_{\text{hjb}} \alpha g_{\text{hjb}}$ 
21:   Update model parameters  $\theta$  with  $s_{\text{opt}}(g)$ 
22:   EMA update of target model  $\bar{s}$ 
23: end for

```

---

## 5 Experiments

In this section, we evaluate our method on a series of distribution matching tasks with non-trivial geometries. In Section 5.2, we compare HOTA with state-of-the-art baselines, demonstrating its superior performance on both standard benchmarks including datasets with almost non-differentiable potentials. In Section 5.3, we demonstrate the scalability of our approach by showcasing its effectiveness in high-dimensional settings. Finally, in Section 5.5, we ablate key components of our method.

### 5.1 Experimental Setup

**Evaluation** We assess performance using two metrics: *feasibility* and *optimality*. Feasibility reflects how well the method matches the target distribution, evaluated via Wasserstein distance with squared Euclidean cost ( $W_2(T_\# \alpha, \beta)$ ), where the transport mapping  $T$  uses optimized value function  $s_\theta$  and samples  $x_1$  by procedure (12). Optimality measures the quality of the resulting mapping, estimated through the integral trajectory cost:  $\int_0^1 \left[ \mathbb{E}_{\rho_t} \frac{\|v_t(x_t)\|^2}{2} + U(x_t) \right] dt$ , where  $x_t$  follows (1).

**Network** In all our experiments, we employ a simple MLP augmented with Fourier feature encoding of the time component. For general time embeddings of the form  $\text{emb}(t) = \sin(f \cdot t + \varphi)$ , the time derivative is given by  $\partial_t \text{emb}(t) = f \cdot \cos(f \cdot t + \varphi)$ . As the frequency  $f$  increases, the magnitude of this derivative also grows, potentially leading to numerical instability—especially when the time derivative of the network is explicitly involved in the objective. This issue has been previously discussed in [Lu and Song \[2024\]](#). To address this, we restrict the frequency range to  $[1, 20]$  and normalize the resulting Fourier features by dividing by the corresponding frequencies.

**Baselines** We use source code from [GSBM repository](#) for running it in our experiments on BabyMaze, Slit and Box datasets. Other results were taken from the original papers [Liu et al. \[2024\]](#), [Pooladian et al. \[2024\]](#) where dataset were previously introduced.

All experiments are conducted on a GeForce RTX 3090 GPU and take less than ten minutes for training. Additional experimental details are provided in [Appendix A](#).

## 5.2 Comparative Evaluation on Two-Dimensional Data

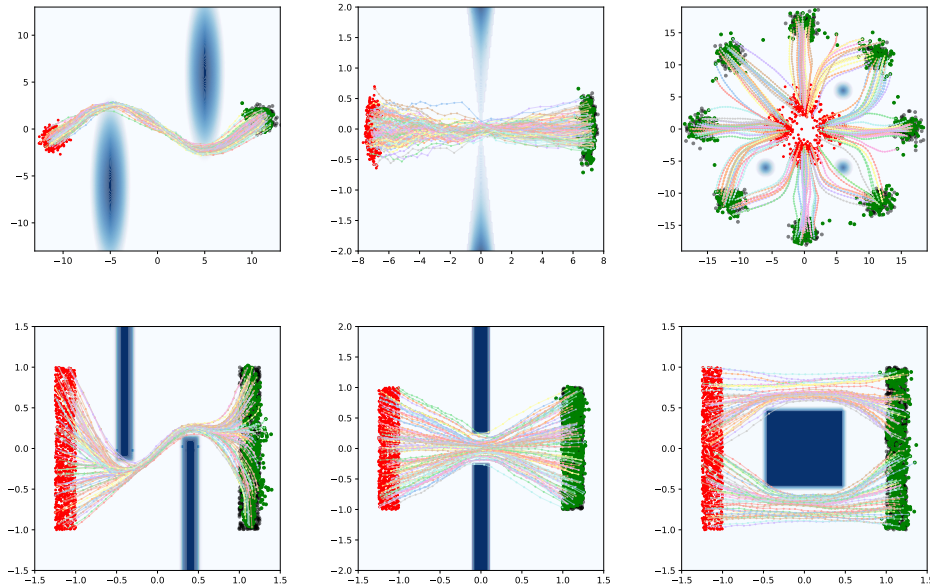


Figure 1: Evaluation of HOTA method on smooth (top) and non-smooth datasets (bottom): Stunnel, Vneck, GMM, BabyMaze, Slit, Box. Blue regions indicate high values of potential  $U(x)$ . Distributions  $\alpha$  (red),  $\beta$  (black) and the mapped  $T_{\#}\alpha$  (green).

In this section, we compare our method to previous state-of-the-art approaches on the standard benchmarks including datasets that feature almost non-differentiable potential functions. Visualizations of the datasets are provided in [Figure 1](#). The first three datasets—Stunnel, Vneck, and GMM—are adopted from [Liu et al. \[2024\]](#). These benchmarks incorporate state cost functions  $U(x_t)$  that encourage the optimal solution to respect complex geometric constraints. Each dataset is designed to highlight specific capabilities of the evaluated algorithms. *Stunnel* assesses whether a method can capture drift fields that undergo rapid and localized changes. *Vneck* evaluates the ability to model drift that compresses and expands the support of marginal distributions. *GMM* tests whether the method can disambiguate closely situated points and assign them to distinct trajectories. The remaining datasets—BabyMaze, Slit, and Box ([Pooladian et al. \[2024\]](#))—are constructed using similar underlying principles but pose additional difficulties due to the presence of almost non-differentiable state cost functions. A summary of the quantitative results across all datasets is provided in [Table 1](#). Our method, HOTA, consistently outperforms existing approaches in terms of both feasibility and optimality. In particular, HOTA achieves a substantial performance gain on the GMM dataset, which may refer to its superior capability in trajectory separation for closely situated points.

Table 1: Quantitative comparison between recent state-of-the-art methods and our approach, HOTA. Performance is evaluated using two criteria: *Feasibility* (how well the target distribution is covered) and *Optimality* (efficiency of the learned mapping). Our method consistently outperforms existing approaches, with significantly better results in certain tasks, such as GMM. N/A cells indicate that original authors of particular method did not include results for those tasks. The mean and the standard deviations of our method are computed across 5 different seeds. Best values are highlighted by bold font (lower is better). Gray values correspond to the method’s divergence.

	Feasibility $W_2(T_\#(\alpha), \beta)$			Optimality (integral cost)		
	Stunnel	Vneck	GMM	Stunnel	Vneck	GMM
NLSB	30.54	0.02	67.76	207.06	147.85	4202.71
GSBM	0.03	0.01	4.13	460.88	155.53	229.12
<b>HOTA</b>	<b><math>0.006 \pm 0.003</math></b>	<b><math>0.002 \pm 0.001</math></b>	<b><math>0.19 \pm 0.05</math></b>	<b><math>320.90 \pm 12.5</math></b>	<b><math>115.09 \pm 8.9</math></b>	<b><math>80.44 \pm 2.6</math></b>
BabyMaze						
NLSB	> 1	0.013	0.024	N/A	N/A	N/A
NLOT	> 1	0.013	0.016	N/A	N/A	N/A
GSBM	0.01	0.01	0.02	6.5	4.9	3.8
<b>HOTA</b>	<b><math>0.004 \pm 0.003</math></b>	<b><math>0.0004 \pm 0.0001</math></b>	<b><math>0.002 \pm 0.001</math></b>	<b><math>4.87 \pm 0.14</math></b>	<b><math>3.06 \pm 0.09</math></b>	<b><math>2.84 \pm 0.11</math></b>

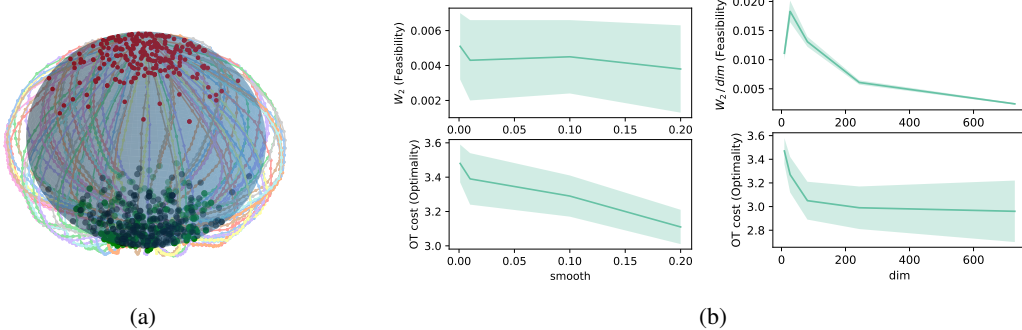


Figure 2: (a) Visualization of *Sphere* dataset for  $N = 3$ . (b) *Feasibility* and *Optimality* trends with respect to 3D unit sphere smoothness (left) and unit sphere dimensionality (right). Our method maintains robust performance across both non-differentiable potentials and high-dimensional settings.

### 5.3 Scalability to High-Dimensional Spaces

In this section, we test the scalability of our method, demonstrating its stable performance in higher-dimensional settings. For this purpose, we use *Sphere* datasets parameterized by data dimensionality  $N$ . Specifically, we define an  $N$ -dimensional unit sphere as a potential barrier inducing corresponding state cost function  $U(x_t)$ . The source and target distributions are samples from a standard distribution located at the poles, projected onto the unit sphere. The three-dimensional case is visualized in Figure 2a. The performance of our method across varying data dimensions is shown in Figure 2b (right). Notably, HOTA demonstrates robust and stable performance as the dimensionality  $N$  increases.

### 5.4 High-dimensional opinion depolarization

Our model employs the polarization mechanism from Liu et al. [2022], which builds on the framework of the political parties introduced by Gaitonde J. [2021]. During each iteration  $t$ , every agent observes a shared random stimulus  $\xi_t \in \mathbb{R}^{1000}$  drawn independently from the current opinion distribution  $p_t$ . The agents then update their positions according to the following response function:

$$f_{\text{polarize}}(x; p_t, \xi_t) = \mathbb{E}_{y \sim p_t} \left[ a(x, y, \xi_t) \cdot \frac{y}{\|y\|^{1/2}} \right], \quad (18)$$

$$a(x, y, \xi_t) = \begin{cases} 1 & \text{if } \text{sign}(x^T \xi_t) = \text{sign}(y^T \xi_t) \\ -1 & \text{if opinions differ,} \end{cases} \quad (19)$$

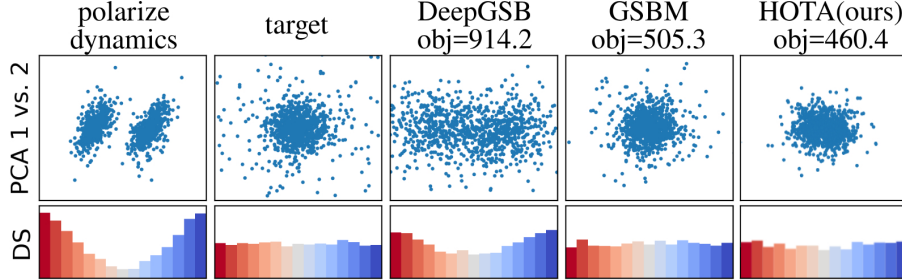


Figure 3: Opinion prediction in dimension 1000 and correspondent directional similarities (DS). Polarize dynamics is the opinion distribution formed without control. The target measure  $\beta$  is multivariate Gaussian with mean 0 and standard deviation  $4I$ .

where the alignment function  $s(x, y, \xi_t)$  quantifies whether agents  $x$  and  $y$  evaluate the information  $\xi_t$  consistently. This formulation captures the psychological tendency that individuals gravitate toward aligned viewpoints while resisting opposing perspectives, ultimately leading to group polarization. In this case, we consider the stochastic process with polarization drift:

$$dx_t = v(t, x_t)dt + f_{\text{polarize}}(x_t; p_t, \xi_t)dt + \sigma dW,$$

where  $\sigma = 0.5$ . The control task is to depolarize the final distribution  $x_1$  and match with the target measure  $\beta = \mathcal{N}(0, 4I)$ , starting from  $x_0 \sim \mathcal{N}(0, \text{diag}(4.0, 0.25, \dots, 0.25))$ . The optimization *objective* here is

$$\int_0^1 \frac{\|v(t, x_t)\|^2}{2} dt. \quad (20)$$

In this experiment, we compare HOTA with the baseline methods DeepGSB Liu et al. [2022] and GSBM Liu et al. [2024]. Following established practices in opinion dynamics research Schweighofer S. [2020], we analyze the distribution of angular separations between opinion vectors (directional similarities). A more uniform angular distribution indicates reduced polarization, while peaked distributions suggest stronger factional divisions. The comparison in terms of task objective (20) and directional similarities is presented in Figure 3.

### 5.5 Ablation study

Table 2 presents comparison of the full HOTA model against variants without the replay buffer  $\mathcal{B}$  that stores simulation history or the adaptive gradient balancing by means of  $\alpha$  (17), evaluating as previously feasibility and optimality metrics across Stunnel, Vneck, and GMM datasets. The full HOTA achieves strong metric scores, while removing the buffer severely degrades feasibility in Vneck and GMM and increases costs in Stunnel. Disabling gradient balancing harms feasibility in Stunnel and GMM. The results highlight the buffer’s critical role in maintaining feasibility and the nuanced trade-offs between gradient balancing and transport efficiency across different scenarios.

Additionally, we have evaluated the influence of the balancing coefficient  $\lambda_{\text{hjb}}$  and the acceleration term  $\lambda_a |a|$  in the loss  $L_{\text{hjb}}$ . The latter penalizes changes in angular velocity to straighten trajectories—our results show that increasing  $\lambda_a$  improves trajectory optimality while introducing a slight bias in matching the target distribution  $\beta$ , as reflected in the feasibility metric. In the GMM task, due to the specificity of the dataset and the divergence of trajectories in different directions, a small penalization of acceleration also improves feasibility. Simultaneously, we optimize the losses  $L_{\text{pot}}$  and  $L_{\text{hjb}}$ , scaling the HJB-loss gradients for stability before summing them with the POT-loss gradients, and we investigate the sensitivity of learning to  $\lambda_{\text{hjb}}$  and its impact on performance in the Stunnel and GMM tasks (Figure 4).

## 6 Limitations and Future Work

While HOTA exhibits strong and robust performance, we observed sensitivity to certain network design choices—particularly the Fourier feature encoding of time, a commonly used technique in models that estimate ODE drifts. Additionally, because the value function in our framework must simultaneously support optimal control estimation and serve as a Kantorovich potential, it requires a network architecture capable of aggregating rich temporal and spatial information. The use of a simple MLP, while effective, may not be optimal from an optimization standpoint. Incorporating

Table 2: Comparison of HOTA method against variants without the replay buffer  $\mathcal{B}$  and the adaptive gradient balancing. Best values are highlighted by bold font (lower is better). Gray values correspond to the method’s divergence.

	Feasibility $W_2(T_\#(\alpha), \beta)$			Optimality (integral cost)		
	Stunnel	Vneck	GMM	Stunnel	Vneck	GMM
HOTA	<b>0.006</b>	<b>0.002</b>	<b>0.19</b>	<b>320.90</b>	115.09	<b>80.44</b>
HOTA w/o buffer	0.076	16.47	1.248	706.89	82.49	121.6
HOTA w/o grad. balancing	3.60	0.026	2.64	325.22	<b>109.25</b>	72.77

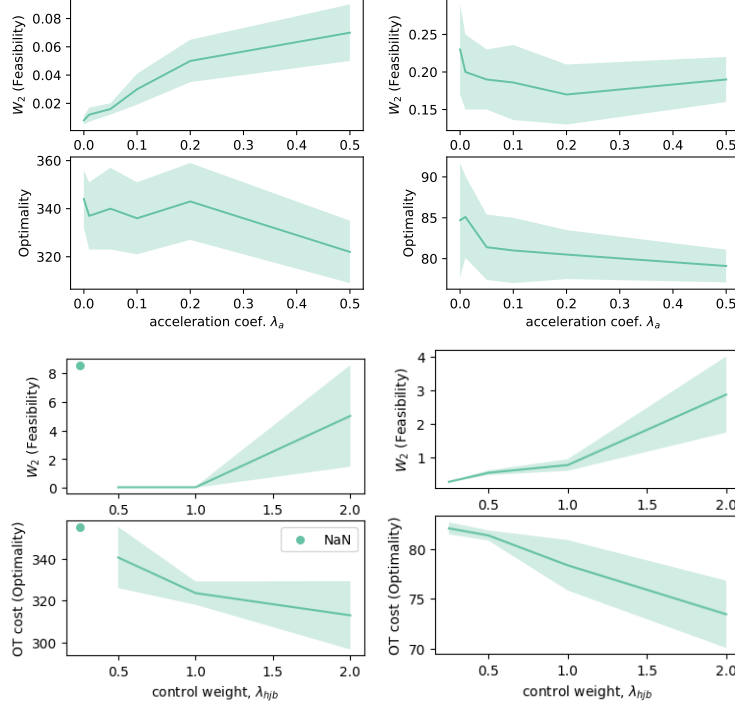


Figure 4: Impact of acceleration coefficient  $\lambda_a$  and control weight  $\lambda_{hjb}$ . Left: Stunnel, right: GMM datasets. The results show a tradeoff: increasing  $\lambda_a$  or  $\lambda_{hjb}$  improves optimal transport (OT) cost but reduces feasibility. Additionally, larger instability arises for both excessively low and high values of  $\lambda_{hjb}$ .

architectures with stronger inductive biases could further enhance performance. These considerations lie beyond the scope of this work, but we believe they offer promising directions for future research.

## 7 Conclusion

In this work, we introduced HOTA, a new OT method based on the Hamilton–Jacobi–Bellman (HJB) framework for solving the Generalized Schrödinger Bridge problem. We demonstrated that HOTA consistently outperforms recent state-of-the-art methods on standard benchmarks and scales effectively to high-dimensional settings. Remarkably, it works for non-smooth potentials and with non-differentiable cost functions, yielding robust performance gain in terms of strictly defined concepts of feasibility and optimality.

## References

- Arip Asadulaev, Rostislav Korst, Aleksandr Korotin, Vage Egiazarian, Andrey Filchenkov, and Evgeny Burnaev. Rethinking optimal transport in offline reinforcement learning. *Advances in Neural Information Processing Systems*, 37:123592–123607, 2024.
- Grigory Bartosh, Dmitry P Vetrov, and Christian Andersson Naesseth. Neural flow diffusion models: Learnable forward process for improved diffusion modelling. *Advances in Neural Information Processing Systems*, 37:73952–73985, 2024.
- Jean-David Benamou and Yann Brenier. A computational fluid mechanics solution to the monge-kantorovich mass transfer problem. *Numerische Mathematik*, 84(3):375–393, 2000.
- Denis Blessing, Julius Berner, Lorenz Richter, and Gerhard Neumann. Underdamped diffusion bridges with applications to sampling. In *The Thirteenth International Conference on Learning Representations*, 2025. URL <https://openreview.net/forum?id=Q1QTxFm0Is>.
- Maksim Bobrin, Nazar Buzun, Dmitrii Krylov, and Dmitry V Dylov. Align your intents: Offline imitation learning via optimal transport. *arXiv preprint arXiv:2402.13037*, 2024.
- Nicolas Bonneel and Julie Digne. A survey of optimal transport for computer graphics and computer vision. *Computer Graphics Forum*, 42(2):439–460, 2023. doi: <https://doi.org/10.1111/cgf.14778>. URL <https://onlinelibrary.wiley.com/doi/abs/10.1111/cgf.14778>.
- Charlotte Bunne, Laetitia Papaxanthos, Andreas Krause, and Marco Cuturi. Proximal optimal transport modeling of population dynamics. In Gustau Camps-Valls, Francisco J. R. Ruiz, and Isabel Valera, editors, *Proceedings of The 25th International Conference on Artificial Intelligence and Statistics*, volume 151 of *Proceedings of Machine Learning Research*, pages 6511–6528. PMLR, 28–30 Mar 2022. URL <https://proceedings.mlr.press/v151/bunne22a.html>.
- Nazar Buzun, Maksim Bobrin, and Dmitry V Dylov. Expectile regularization for fast and accurate training of neural optimal transport. *Advances in Neural Information Processing Systems*, 37:119811–119837, 2024.
- Marco Cuturi. Sinkhorn distances: Lightspeed computation of optimal transport. *Advances in neural information processing systems*, 26, 2013.
- Carles Domingo-Enrich, Michal Drozdzal, Brian Karrer, and Ricky TQ Chen. Adjoint matching: Fine-tuning flow and diffusion generative models with memoryless stochastic optimal control. *arXiv preprint arXiv:2409.08861*, 2024a.
- Carles Domingo-Enrich, Jiequn Han, Brandon Amos, Joan Bruna, and Ricky T. Q. Chen. Stochastic optimal control matching. In *The Thirty-eighth Annual Conference on Neural Information Processing Systems*, 2024b. URL <https://openreview.net/forum?id=wfU2CdgmWt>.
- Wendell H. Fleet and H. Mete Soner. Controlled markov processes and viscosity solutions (2nd ed.). *Springer*, 2006.
- Tardos E. Gaitonde J., Kleinberg J. Polarization in geometric opinion dynamics. *Proceedings of the ACM Conference on Economics and Computation*, 2021.
- Kacper Kapusniak, Peter Potapchik, Teodora Reu, Leo Zhang, Alexander Tong, Michael Bronstein, Joey Bose, and Francesco Di Giovanni. Metric flow matching for smooth interpolations on the data manifold. *Advances in Neural Information Processing Systems*, 37:135011–135042, 2024.
- Pascal Klink, Haoyi Yang, Carlo D’Eramo, Jan Peters, and Joni Pajarinen. Curriculum reinforcement learning via constrained optimal transport. In Kamalika Chaudhuri, Stefanie Jegelka, Le Song, Csaba Szepesvari, Gang Niu, and Sivan Sabato, editors, *Proceedings of the 39th International Conference on Machine Learning*, volume 162 of *Proceedings of Machine Learning Research*, pages 11341–11358. PMLR, 17–23 Jul 2022. URL <https://proceedings.mlr.press/v162/klink22a.html>.
- Alexander Korotin, Daniil Selikhnovych, and Evgeny Burnaev. Neural optimal transport. *arXiv preprint arXiv:2201.12220*, 2022.
- Sergey Levine. Reinforcement learning and control as probabilistic inference: Tutorial and review. *CoRR*, abs/1805.00909, 2018.
- Yaron Lipman, Ricky T. Q. Chen, Heli Ben-Hamu, Maximilian Nickel, and Matthew Le. Flow matching for generative modeling. In *The Eleventh International Conference on Learning Representations*, 2023.
- Guan-Horng Liu, Tianrong Chen, Oswin So, and Evangelos A Theodorou. Deep generalized schrödinger bridge. In *Advances in Neural Information Processing Systems*, 2022.
- Guan-Horng Liu, Yaron Lipman, Maximilian Nickel, Brian Karrer, Evangelos Theodorou, and Ricky T. Q. Chen. Generalized schrödinger bridge matching. In *The Twelfth International Conference on Learning Representations*, 2024.
- Cheng Lu and Yang Song. Simplifying, stabilizing and scaling continuous-time consistency models. 2024.
- Ashok Makkluva, Amirhossein Taghvaei, Sewoong Oh, and Jason Lee. Optimal transport mapping via input convex neural networks. In *International Conference on Machine Learning*, pages 6672–6681. PMLR, 2020.

- Eduardo Fernandes Montesuma, Fred Maurice Ngole Mboula, and Antoine Souloumiac. Recent advances in optimal transport for machine learning. *IEEE Transactions on Pattern Analysis and Machine Intelligence*, 2024.
- Benjamin Nachman Nathan T. Suri, Vinicius Mikuni. Wotan: Weakly-supervised optimal transport attention-based noise mitigation. *NeurIPS 2024*, 2024.
- Kirill Neklyudov, Rob Brekelmans, Alexander Tong, Lazar Atanackovic, Qiang Liu, and Alireza Makhzani. A computational framework for solving Wasserstein lagrangian flows. In Ruslan Salakhutdinov, Zico Kolter, Katherine Heller, Adrian Weller, Nuria Oliver, Jonathan Scarlett, and Felix Berkenkamp, editors, *Proceedings of the 41st International Conference on Machine Learning*, volume 235 of *Proceedings of Machine Learning Research*, pages 37461–37485. PMLR, 21–27 Jul 2024.
- Luiz Manella Pereira and M Hadi Amini. A survey on optimal transport for machine learning: Theory and applications. *IEEE Access*, 2025.
- Gabriel Peyré, Marco Cuturi, et al. Computational optimal transport: With applications to data science. *Foundations and Trends® in Machine Learning*, 11(5-6):355–607, 2019.
- Aram-Alexandre Pooladian, Carles Domingo-Enrich, Ricky T. Q. Chen, and Brandon Amos. Neural optimal transport with lagrangian costs. In *The 40th Conference on Uncertainty in Artificial Intelligence*, 2024.
- Thomas Rupf, Marco Bagatella, Nico Görtler, Jonas Frey, and Georg Martius. Zero-shot offline imitation learning via optimal transport, 2025. URL <https://openreview.net/forum?id=vDecbmWf6w>.
- Filippo Santambrogio. *Optimal transport for applied mathematicians*, volume 87. Springer, 2015.
- Schweitzer F. Schweighofer S., Garcia D. An agent-based model of multidimensional opinion dynamics and opinion alignment. *Chaos: An Interdisciplinary Journal of Nonlinear Science*, 2020.
- Evangelos Theodorou, Jonas Buchli, and Stefan Schaal. Learning policy improvements with path integrals. In Yee Whye Teh and Mike Titterington, editors, *Proceedings of the Thirteenth International Conference on Artificial Intelligence and Statistics*, volume 9 of *Proceedings of Machine Learning Research*, pages 828–835, Chia Laguna Resort, Sardinia, Italy, 13–15 May 2010. PMLR.
- Cédric Villani et al. *Optimal transport: old and new*, volume 338. Springer, 2008.

## A Additional Experimental Details

**Hyperparameters** Table 3 summarizes the hyperparameters used for each dataset presented in the paper. Note that the Sphere datasets, which are parameterized by data dimensionality, share all hyperparameters except for the potential weight, which may take value 10 for the low dimensions and 30 for high ones.

Table 3: Hyperparameters used for each dataset presented in the paper.

Hyperparameter	Stunnel	Vneck	GMM	BabyMaze	Slit	Box	Sphere
MLP hidden layers				[512, 512, 512, 1]			
Fourier frequencies				{1, ..., 20}			
optimizer				Adam with cosine annealing ( $\alpha = 1e-2$ )			
initial learning rate				$5 \times 10^{-4}$			
Adam $[\beta_1, \beta_2]$				[0.9, 0.99]			
# training iterations				70000			
batch size				1024			
EMA decay, $\tau$				0.9			
# control steps				30			
diffusion coef., $\sigma$	0.3	0.2	0.1	0.03	0.05	0.03	0.01
control weight, $\lambda_a$	1.0	2.0	0.7	0.5	2.0	0.3	0.4
acc. weight, $\lambda_a$	0.0001	0.001	0.2	0.05	0.001	0.01	0
potential weight	25	1000	25	10	30	700	{10, 30}

## B Proof of Theorem 1 (Dual Formulation of GSB)

We prove in the **first step** the equivalence between the GSB (stochastic control formulation) and its dual formulation using Kantorovich-style duality. Remind that we consider the stochastic process  $x_t$  (1) with conditions  $x_0 \sim \alpha$ ,  $x_1 \sim \beta$ , control function  $v(t, x_t)$ , and Brownian motion  $\sigma(t, x_t) dW_t$ . The **primary problem** of GSB optimization is:

$$\inf_{v(t,x)} \mathbb{E} \left[ \int_0^1 \mathcal{L}(t, x_t, v_t) dt \right] \quad \text{s.t.} \quad x_0 \sim \alpha, x_1 \sim \beta, \quad (21)$$

where in the particular case  $\mathcal{L}(t, x, v) = v^2/2 + U(x)$ . Since the stochastic process  $x_t$  starts from  $x_0 \sim \alpha$  the primal problem is equivalent to:

$$\inf_{v(t,x)} \left( \mathbb{E} \left[ \int_0^1 \mathcal{L}(t, x_t, v_t) dt \right] + \sup_{g \in L_1(\beta)} (-\mathbb{E}[g(x_1)] + \mathbb{E}_\beta[g(y)]) \right), \quad (22)$$

where the supremum over  $g$  enforces the constraint  $x_1 \sim \beta$  (via Lagrange duality). Rewrite the Lagrangian problem as

$$\inf_{v(t,x)} \sup_{g \in L_1(\beta)} \left( \mathbb{E} \left[ \int_0^1 \mathcal{L}(t, x_t, v_t) dt - g(x_1) \right] + \mathbb{E}_\beta[g(y)] \right). \quad (23)$$

Assuming strong duality holds under mild regularity conditions (e.g.,  $\mathcal{L}$  convex in  $v$ ,  $\alpha, \beta$  absolutely continuous), we swap inf and sup:

$$\sup_{g \in L_1(\beta)} \left( \inf_{v(t,x)} \mathbb{E} \left[ \int_0^1 \mathcal{L}(t, x_t, v_t) dt - g(x_1) \right] + \mathbb{E}_\beta[g(y)] \right). \quad (24)$$

Note that since the optimal  $v^*(t, x)$  is Markovian (depends only on current time  $t$  and state  $x$ ) and does not depend on the initial distribution  $\alpha$  it holds that

$$\mathbb{E} \left[ \int_0^1 \mathcal{L}(t, x_t, v_t^*) dt - g(x_1) \right] = \mathbb{E}_{x \sim \alpha} \mathbb{E} \left[ \int_0^1 \mathcal{L}(t, x_t, v_t^*) dt - g(x_1) \mid x_0 = x \right]. \quad (25)$$

Buy the definition of  $c$ -conjugate transform (5):

$$\mathbb{E}_{x \sim \alpha} \mathbb{E} \left[ \int_0^1 \mathcal{L}(t, x_t, v_t^*) dt - g(x_1) \mid x_0 = x \right] = \mathbb{E}_{x \sim \alpha} g^c(x). \quad (26)$$

Thus, the **dual problem** becomes:  $\sup_{g \in L_1(\beta)} (\mathbb{E}_\alpha[g^c(x)] + \mathbb{E}_\beta[g(y)])$ . In the **second step** find the optimal control solution  $v^*(t, x)$  by means of dynamic programming principle. Define the value function  $s(t, x)$  that for any  $0 \leq t \leq \tau \leq 1$  satisfies:

$$s(t, x) = \inf_{v(t, x)} \mathbb{E} \left[ \int_t^\tau \mathcal{L}(z, x_z, v_z) dz + s(\tau, x_\tau) \mid x_t = x \right]. \quad (27)$$

Applying Ito's formula to  $s(\tau, x_\tau)$  we obtain that

$$ds(\tau, x_\tau) = \partial_\tau s d\tau + \nabla s \cdot dx_\tau + \frac{1}{2} \text{tr}(\sigma^2 \nabla^2 s) d\tau \quad (28)$$

$$= \left( \partial_\tau s + \nabla s^T v_\tau + \frac{1}{2} \text{tr}(\sigma^2 \nabla^2 s) \right) d\tau + \nabla s^T \sigma dW_s. \quad (29)$$

Consider the evolution of the value between times  $t$  and  $\tau$ :

$$s(\tau, x_\tau) - s(t, x_t) = \int_t^\tau \left( \partial_z s + \nabla s \cdot v_z + \frac{1}{2} \text{tr}(\sigma^2 \nabla^2 s) \right) dz + \int_t^\tau \nabla s^T \sigma dW. \quad (30)$$

Basing on the martingale property of Ito integrals ( $\mathbb{E}[\int \nabla s \cdot \sigma dW \mid x_t = x] = 0$ ) it holds that

$$\mathbb{E}[s(\tau, x_\tau) \mid x_t = x] = s(t, x) + \mathbb{E} \left[ \int_t^\tau \left( \partial_z s + \nabla s \cdot v_z + \frac{1}{2} \text{tr}(\sigma^2 \nabla^2 s) \right) dz \right]. \quad (31)$$

Substitute back into dynamic programming and plug the last expression into the equation (27):

$$s(t, x) = \inf_{v(t, x)} \mathbb{E} \left[ \int_t^\tau \mathcal{L}(z, x_z, v_z) dz + s(t, x) + \int_t^\tau \left( \partial_z s + \nabla s^T v_\tau + \frac{1}{2} \text{tr}(\sigma^2 \nabla^2 s) \right) dz \right]. \quad (32)$$

Cancel  $s(t, x)$  from both sides and divide by  $(\tau - t)$ :

$$0 = \inf_{v(s, t)} \frac{1}{\tau - t} \mathbb{E} \left[ \int_t^\tau \left( \mathcal{L}(z, x_z, v_z) + \partial_z s + \nabla s^T v_z + \frac{1}{2} \text{tr}(\sigma^2 \nabla^2 s) \right) dz \right]. \quad (33)$$

Take limit  $\tau \downarrow t$  to derive the HJB equation for a general Lagrangian  $\mathcal{L}$

$$0 = \inf_v \left\{ \mathcal{L}(t, x, v) + \partial_t s + \nabla s^T v + \frac{1}{2} \text{tr}(\sigma^2 \nabla^2 s) \right\}. \quad (34)$$

Identify optimal control for the particular  $\mathcal{L}(t, x, v) = v^2/2 + U(x)$ . The infimum is attained when  $v^* = -\nabla s$ , yielding the final result of Theorem 1.